Journal of Mechanical Engineering Research and Developments
ISSN: 1024-1752
CODEN: JERDFO
Vol. 43, No.6, pp. 418-439
Published Year 2020

Natural Convection in Eccentric Annuli packed with Spheres

Ayad K. Hassan[†], Ali Abd Al-Nabi Abaas[‡], Salman H. Omran[‡†], Laith Jaafer Habeeb[‡‡]

[†]University of Technology, Materials Engineering Department, Baghdad, Iraq.
[‡]Mustansiriya University, Government Contracts Division, Baghdad, Iraq.
[‡†]University of Technology, Energy and Renewable Energies Technology Center, Baghdad, Iraq.
[‡‡]University of Technology, Training and Workshop Center, Baghdad, Iraq.

*Corresponding Author Email: Ayad_kadhm@yahoo.com; tripleali_71@yahoo.com; asst.prof.salman@gmail.com; laithhabeeb1974@gmail.com

ABSTRACT: A numerical investigation of two-dimensional natural convection about a horizontal circular heated cylinder embedded in cylindrical packed bed of spheres under the condition of local thermal non-equilibrium is reported. The present parametric investigation concentrates on the use of two-phase energy model (local thermal non-equilibrium *LTNE*), which does not consider the condition of thermal equilibrium between the flowing fluid and the solid spheres, to predict the thermal characteristics and the heat transfer rates within the annuli. The investigation is conducted for a constant cylinder-to-particle diameter ratio (Di/d) = 30, porosity (ε) = 0.5, and solid/fluid thermal conductivity ratio (k_R) = 1.0. The effects of three annular eccentricities (e = 0, -0.8, 0.8) on the rates of heat transfer throughout both the fluid Nu_f and solid Nu_s phases are examined for various Rayleigh numbers ($Ra = 10^4$ - 5×10^7). The results show that the increase in Rayleigh number has a considerably positive impact on Nu_f ; however, Nu_s is hardly affected by increasing it. In addition, a significant increase in Nu_f can be obtained by moving the inner cylinder towards the bottom of the outer cylinder.

KEYWORDS: Natural convection, Laminar flow, Annular enclosure, Porous medium, Concentric

INTRODUCTION

Natural convection heat transfer in annuli takes place in numerous industrial applications such as within the nuclear, solar, and thermal storage systems, as well as in the different electric energy fields. The presence of a fluid between two circular cylinders, concentric or eccentric, at different fixed temperatures generates a complicated buoyancy-driven flow in the existence of a constant gravitational force. If the temperature discrepancy between the cylinders is, slight, the energy conveyance will be dominated by diffusion. Therefore, the average Nusselt number stays generally invariable in such conductive flow regime for the entire Rayleigh numbers under a specific critical value. Over this critical Rayleigh number, the thermal convection occurs producing thermal plumes appearing in the annular gap. Natural convection inside annular spaces has been analyzed extensively, and received much attention in the literature. For example, the authors [1-5] investigated this problem in concentric annuli; while others such as [6-15] focused on the influence of eccentricity on heat transfer for various boundary conditions and using different numerical methods.

Briefly, Kuehn and Goldstein [6] developed a correlation to predict natural convection heat transfer from horizontal cylinder to a fluid inside a cylindrical enclosure under quasi-steady conditions using a conduction boundary-layer model. Ratzel et al. [7] examined free convection in concentric and eccentric annular areas using a finite element procedure. Yao [8] studied analytically free convection in eccentric annuli employing perturbation techniques. Natural convective flows in eccentric annuli were studied numerically by Projahn et al. [9] employing the implicit finite difference method with the body-fitted curvilinear coordinate transformations. They reported results for both vertical and horizontal eccentricities were compared with the results presented by Kuehn and Goldstein [6]. The bipolar coordinate transformations were also utilized by Feldman et al. [10] to estimate the developing flow and thermal fields within an eccentric annular vertical duct. Darrell and Roger [11] studied numerically free convection heat transfer inside an eccentric annular gap between two circular cylinders isothermally heated employing the one-dimensional finite element method with a bipolar coordinate transformation and pseudospectral algorithms. Ho et al. [12] investigated free convection heat transfer in eccentric annuli with mixed boundary conditions and presented a correlation for the Nusselt number against Rayleigh number. Hwang and Jensen [13] studied the convective laminar dispersed flow in an eccentric annulus using the separation of variables method. Koichi et al. [14] examined natural convection heat transfer in eccentric horizontal annuli between a heated outer elliptical tube and a cooled inner cylindrical tube with different orientations. Hosseini et al. [15] investigated free convection in an open-ended vertical eccentric annulus, and observed there is best possible value of eccentricity with a maximum heat removal.

Natural convection inside cylindrical porous annuli has a great importance in many industrial applications such as underground cable systems, thermal energy storages, and thermal insulations. The case of concentric porous annulus has obtained the much focus in the literature. Caltagirone [16] conducted the first experimental investigation on porous annulus of constant radius ratio employing the Christiansen effect to picture the isotherms in a cylindrical porous layer. Caltagirone was able to observe only bicellular flow regime, and therefore he concluded that the multicellular structures do not exist when Rayleigh number increases. Later, Fukuda et al. [17] presented three-dimensional results for an inclined annulus using the finite difference method. Rao et al. [18, 19] studied the horizontal annulus in both two and three dimensions employing the Galerkin method. Himasekhar and Bau [20] studied the behavior of bifurcation phenomena using the regular perturbation expansion techniques and the Galerkin method. The visualization experiments of Caltagirone [16] have been re-conducted by Charrier-Mojtabi et al. [21] who proved the presence of two-dimensional four-cell flow structures. Numerical works done by Barbosa Mota and Saatdjian [22,24] examined the effect of radius ratio on the transition of the flow regime and its stability. They showed that the transition from a two-cell to a four-cell flow system relies on Rayleigh number, whether it increases or decreases.

The decrease in the heat transfer by utilizing an eccentric geometry was first examined numerically by Bau et al. [25] employing the finite difference technique, and by Bau, H. H [26] using the regular perturbation expansion technique. In a later work, Himasekhar, K. and Bau, H. H [27] utilized a boundary-layer technique to formulate a correlation for Nusselt number with Rayleigh number and geometrical parameters. In these works, the flow pattern was restricted to just the two-dimensional bicellular one, which is obviously not the only flow pattern that can take place in reality. Barbosa Mota and Saatdjian [28] who considered the four-cellular flow conditions in an eccentric cylinder, found out that the eccentricity that reduces the heat loss for particular radius ratio and Rayleigh number can considerably alter the flow system. Barbosa Mota et al. [29] studied natural convection heat transfer in an elliptic annulus containing saturated porous media using a high-order compact finite difference technique.

To the authors' knowledge, all the published articles abovementioned have employed the simple Darcy-Boussinesq model with the thermal equilibrium assumption. The present study is to extend the previously published work by considering the full Brinkman-Forchheimer-extended Darcy (*BFD*) model for the fluid flow and the Local Thermal non-Equilibrium (*LTNE*) energy model. Indeed, this extension to the *BFD* and the *LTNE* can be considered as a new feature in this study to investigate numerically natural convection heat transfer from a circular horizontal isothermal cylinder fixed inside a cylindrical packed bed of spherical particles. Effect of the cylinder eccentricity for several Rayleigh numbers on the temperature and flow distributions, and the rates of heat removal, will be investigated in detail.

PROBLEM DESCRIPTION

The physical model of the problem under examination is described in Figure 1. As illustrated, a circular inner cylinder of radius (r_i) and wall temperature (T_h) is laid inside a bigger outer cylinder of radius (r_o) and wall temperature (T_c) packed with small spheres of diameter (d). The distance between the centers of the two cylinders represents the annuli eccentricity (e). It is assumed that the inner cylinder wall is abruptly heated to (T_h), and thereafter preserved at that temperature, where $T_h > T_c$, generating a buoyancy-induced laminar flow.

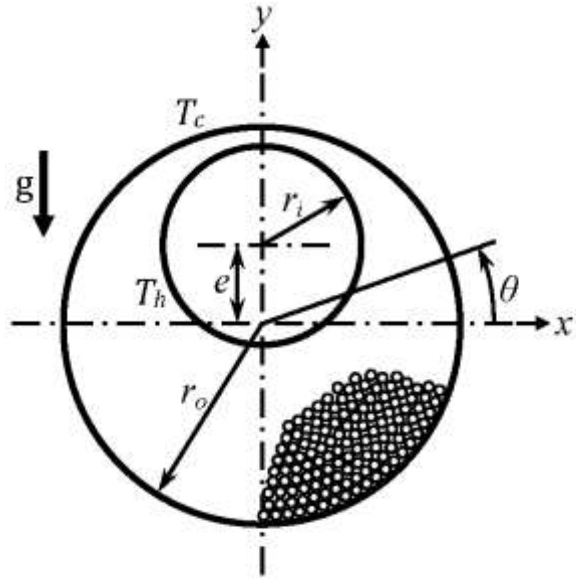

Figure 1. The physical problem.

BASIC EQUATIONS

A two-dimensional natural convection ow of viscous incompressible fluid in an isotropic and homogeneous packed bed of spherical particles is assumed. The full Brinkman-Forchheimer-extended Darcy model with the Boussinesq approximation for the density is used to describe the fluid flow. Importantly, the solid spheres and the fluid are in Local Thermal non-Equilibrium circumstances everywhere, so the two-equations energy model is used to predict the fluid and solid temperatures. With these assumptions, the conservation equations for mass, momentum and energy in the porous medium can be prescribed in the non-dimensional format as follows Vafai and Sozen [30] and Amiri and Vafai[31]:

1. Continuity equation.

$$\frac{\partial u}{\partial y}+\frac{\partial \upsilon}{\partial y}=0 \tag{1}$$

2. X-Momentum equation.

$$\frac{1}{\varepsilon^2}\left(u\frac{\partial u}{\partial x}+\upsilon\frac{\partial u}{\partial y}\right)=-\frac{\Pr}{Da}u-\frac{C_F}{\sqrt{Da}}\left|\vec{u}\right|u+\frac{\Pr}{\varepsilon}(\nabla^2 u)-\frac{\partial P_f}{\partial x} \tag{2}$$

3. Y-Momentum equation.

$$\frac{1}{\varepsilon^2}\left(u\frac{\partial \upsilon}{\partial x}+\upsilon\frac{\partial \upsilon}{\partial y}\right)=-\frac{\Pr}{Da}\upsilon-\frac{C_F}{\sqrt{Da}}\left|\vec{u}\right|\upsilon+\frac{\Pr}{\varepsilon}(\nabla^2 \upsilon)-\frac{\partial P_f}{\partial y}+Ra.\Pr.T_f \tag{3}$$

4. Fluid Energy equation.

$$\varepsilon\left(u\frac{\partial T_f}{\partial x}+\upsilon\frac{\partial T_f}{\partial y}\right)=\nabla.\left(\frac{k_{f.eff}}{k_f}\nabla T_f\right)+Bi.k_R\left(T_s-T_f\right) \tag{4}$$

5. Solid Energy equation.

$$\frac{k_{f.eff}}{k_f}\left(\nabla^2 T_f\right)-Bi\left(T_s-T_f\right)=0 \tag{5}$$

where, the following dimensionless groups are employed:

$$x,y=\frac{x',y'}{D_i},\qquad u=\frac{u'D_i}{\alpha_f},\qquad \upsilon=\frac{\upsilon'D_i}{\alpha_f},\qquad T_f=\frac{\left(T'_f-T'_c\right)}{\left(T'_h-T'_c\right)},\qquad P_f=\frac{pf.D_i^2}{pf\alpha_f^2} \tag{6}$$

where, (u'), (υ') are the dimensional horizontal and vertical velocity components along the dimensional (x') and (y') directions, and (T') and (pf) are the dimensional temperature and pressure. While, (u), (υ) are the dimensionless horizontal and vertical velocity components along the dimensionless (x) and (y) directions, and (T) and (Pf) are the dimensionless temperature and pressure, and (ε) is the porosity. The subscripts (f) and (s) denote the mobile fluid phase and the stationary solid phase, respectively.

The main non-dimensional parameters, i.e., Rayleigh, Darcy, Prandtl, Biot numbers and solid/fluid thermal conductivity ratio, appearing in the above equations can be defined as follows:

$$Ra=\frac{g\beta D_i^3\left(T_h-T_c\right)}{\alpha_f\nu_f},\quad Da=\frac{K}{D_i^2},\quad \Pr=\frac{\nu_f}{\alpha_f},\quad Bi=\frac{D_i^2h_{sf}a_{sf}}{k_s},\quad k_R=\frac{k_s}{k_f} \tag{7}$$

where (ρ_f), (α_f), and (ν_f) are the density, the thermal diffusivity, and the kinematic viscosity, respectively, of the flowing fluid, and (g) and (β) are the gravitational acceleration and the volumetric expansion coefficient. In addition, (k_s) and (k_f) are the solid and fluid thermal conductivities, respectively, and (C_F) and (K) are the inertia coefficient and the permeability, respectively, of the porous medium. The Ergun's empirical expressions Ergun [32] for packed beds of spheres of diameter (d) are employed here to describe (K) and (C_F) as follows:

$$K=\frac{\varepsilon^3d^2}{150(1-\varepsilon)^2},\qquad C_F=\frac{1.75}{\sqrt{150\varepsilon^3}} \tag{8}$$

whereas, (h_{sf}) is the fluid-to-sphere convective heat transfer coefficient and (α_{sf}) is the sphere specific surface area. The correlations of Dullien [33] for (α_{sf}), and by Wakao et al. [34] for (h_{sf}) are used as follows:

$$\alpha_{sf}=\frac{6\left(1-\varepsilon\right)}{d} \tag{9}$$

$$h_{sf}=\frac{k_f}{d}\left(2+\Pr^{1/3}\left(\frac{|u|d}{\nu_f}\right)^{0.6}\right)$$

(10)

The Reynolds number in the sphere level (Re_p) is defined:

$$\mathrm{Re}_p=\frac{|u|d}{\nu_f} \tag{11}$$

In turn, the Biot number Bi can be expressed as:

$$Bi=6\left(1-\varepsilon\right)\left(\frac{1}{k_R}\right)\left(\frac{D_i}{d}\right)^2\left[2+\Pr^{1/3}\left(\mathrm{Re}_p\right)^{0.6}\right] \tag{12}$$

In this investigation, the fluid and solid effective thermal conductivity ($k_{s,eff}$) and ($k_{s,eff}$), respectively, represent the stagnant conductivity of the two phases, which can be calculated based on the experimental correlation of Zehner and Schluender [35] as follows:

$$\frac{k_{st}}{k_f} = \left(1-\sqrt{1-\varepsilon}\right) + \frac{2\sqrt{1-\varepsilon}}{1-\lambda B} \times \left[\frac{(1-\lambda)B}{(1-\lambda B)^2} \ln(\lambda B) - \frac{B+1}{2} - \frac{B-1}{1-\lambda B} \right] \tag{13}$$

$$\frac{k_{s,eff}}{k_s} = (1-\varepsilon) \tag{14}$$

Where $\lambda = 1/k_R$ and $B = 1.25\left[(1-\varepsilon)/\varepsilon\right]^{\frac{10}{9}}$

Boundary conditions

The boundary conditions for the non-dimensional variables:

$$u = \upsilon = 0 \quad at \quad (r = r_i) \quad and \quad (0 < \varphi^o < 360)$$

$$u = \upsilon = 0 \quad at \quad (r = r_o) \quad and \quad (0 < \varphi^o < 360)$$

$$T_f = T_s = 1 \quad at \quad (r = r_i) \quad and \quad (0 < \varphi^o < 360)$$

$$T_f = T_s = 0 \quad at \quad (r = r_o) \quad and \quad (0 < \varphi^o < 360) \tag{15}$$

Calculation of heat transfer

The rates of heat transfer throughout the fluid and solid phases are calculated by applying the Fourier's law at the heated cylinder surface as follows:

$$q_f = -\frac{k_{f,eff}}{k_f} \frac{\partial T_f'}{\partial n}\bigg|_{r=r_i} , \qquad q_s = -\frac{k_{s,eff}}{k_s} \frac{\partial T_s'}{\partial n}\bigg|_{r=r_i} \tag{16}$$

and in terms of the dimensionless variables,

$$Nu_f = \frac{q_f D_i}{\left(T_h - T_f'\right)} = \frac{1}{S}\int_0^S \frac{k_{f,eff}}{k_f} \frac{\partial \theta_f}{\partial n} ds\bigg|_{r=r_i}$$

$$Nu_s = \frac{q_s D_i}{\left(T_h - T_s'\right)} = \frac{1}{S}\int_0^S \frac{k_{s,eff}}{k_s} \frac{\partial T_s}{\partial n} ds\bigg|_{r=r_i} \tag{17}$$

where, t and n refer to the tangential and perpendicular directions at the inner cylinder wall, respectively, while S is the periphery of the inner cylinder, and Nu_f represents the fluid Nusselt number, whereas Nu_s represents the solid Nusselt number. Therefore, the total Nusselt number Nu_t can be expressed as the summation of Nu_f and Nu_s :

$$Nu_t = Nu_f + Nu_s \tag{18}$$

Computational procedure

A nodal spectral-element method described in Fletcher [36], Fletcher [37], and Karniadakis and Sherwin [38] is employed as a tool for discretizing the governing flow and energy equations (1-5) in space. The computational zone is splitted up into a grid of distinct macro-elements. Nevertheless, rather than using a linear low-order basis across every single element, a high-order polynomial basis is utilized, providing a finer mesh of micro-elements, thereby permitting very fast convergence with increasing polynomial degree p_l. The macro- and micro-meshes, which are employed in the present investigation for the annuli eccentricity e = 0.8 shown in Figure 2, use 520 and 33280 elements, respectively. A Grid Resolution Study (GRS) was performed to ensure that the current numerical results are independent to the computational mesh. The resolution of mesh is altered by varying the order of p_l from 3 to 9. Numerical simulations have been made at different parameters. The solid and fluid average Nusselt numbers Nu_s and Nu_f, respectively, were used as an accuracy indication. The results presented in Figure 3 demonstrate that an eighth-order polynomial ($p_l = 8$) can be used to give a relative error of less than 1% in Nu_f and Nu_s.

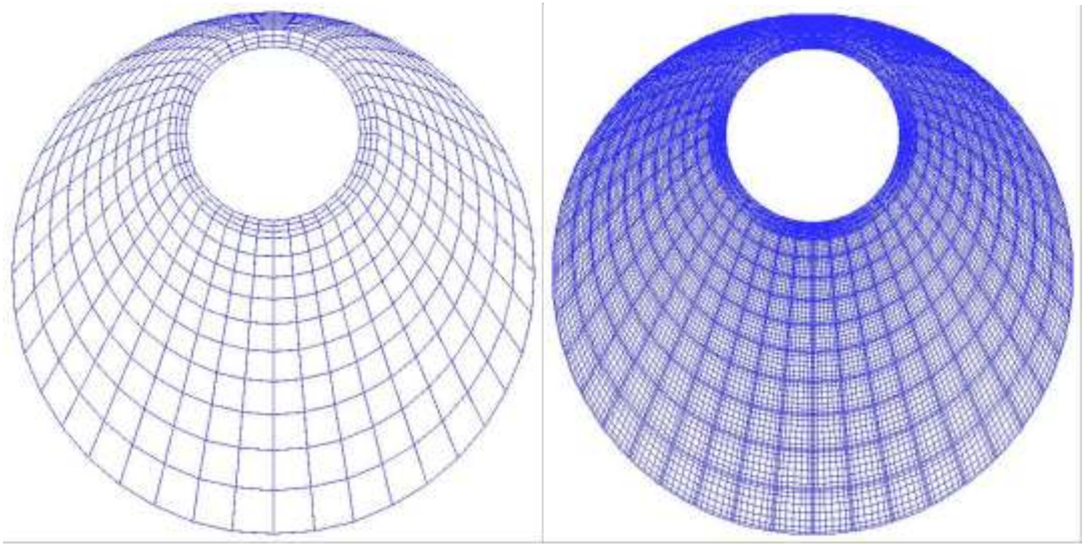

Figure 2. The computational mesh employed at e = 0.8, (Left) macro-mesh, and (Right) micro-mesh.

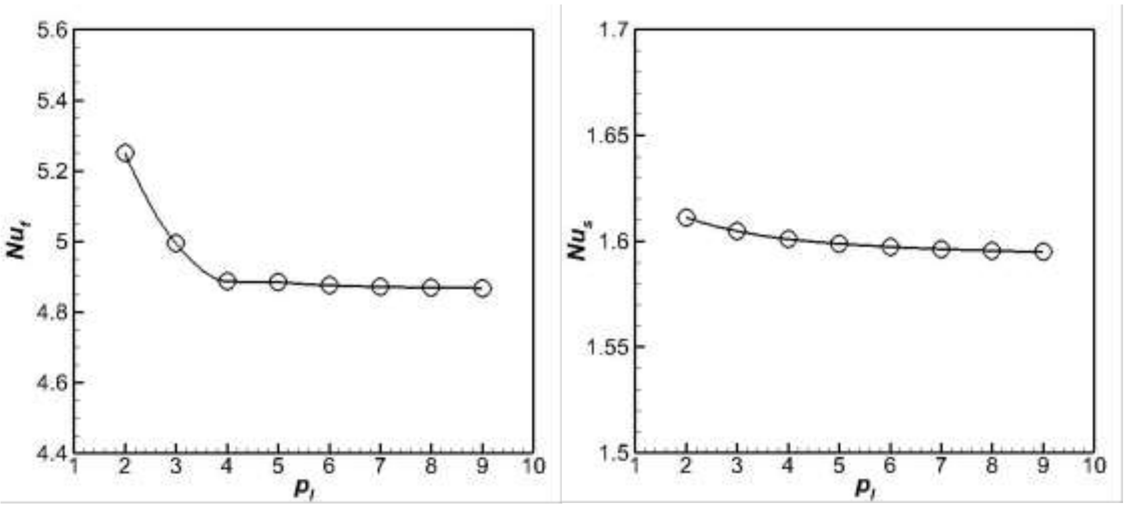

Figure 3. (Left) Fluid, and (Right) solid, average Nusselt numbers distributions with polynomial degree p_l, for the Grid Resolution Study (GRS).

The numerical results of the present in-home FORTRAN program have been validated and compared with those of Buyruk [39] for the case of forced convective flow across a bank of horizontal cylinders. This investigation was made for three staggered cylinders of similar longitudinal and transverse pitches. The cylinders are isothermally heated and placed in a uniform cold air cross flow. Figures 4 illustrates the comparison for the two predictions of temperature patterns over the cylinders for Reynolds number $Re_D = 80$. It can be observed that the comparison demonstrates an acceptable agreement between both numerical solutions.

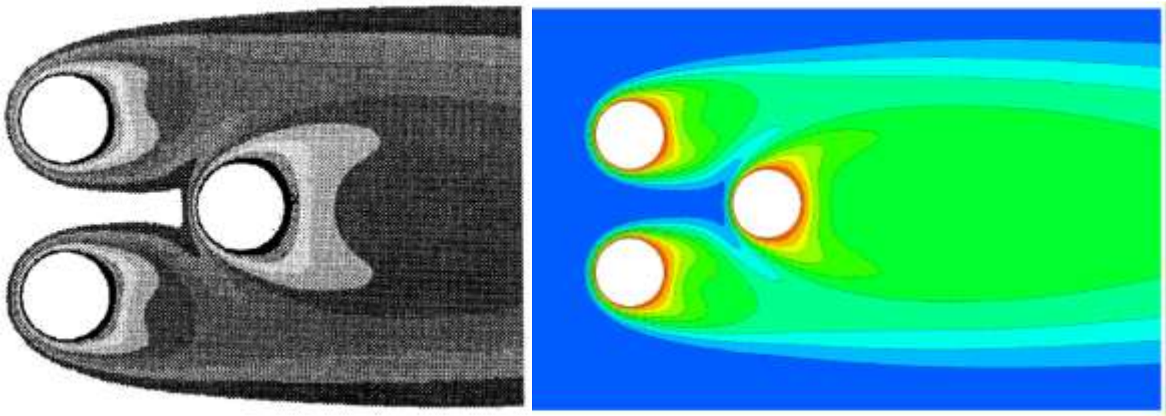

Figure 4. (Right) The numerical results predicted by the present code (Left) the numerical results of Buyruk [39], for temperature distribution across three staggered cylinders.

RESULTS AND DISCUSSION

The present investigation is about natural convection from a heated circular cylinder located in a cylindrical backed bed of spherical beads. The main objective is to examine the effect of a geometric parameter namely; annuli eccentricity (e), on the convective and conductive heat transfer throughout the fluid and solid phases, and more generally on their thermal fields, for several Rayleigh numbers (Ra). The geometric and thermal properties of the porous material are maintained constant, e.g. solid-to-fluid thermal conductivity ratio (k_R) = 1.0, cylinder-to-sphere diameter ratio (D_i/d) = 30, and porosity (ε) = 0.5, and the air being chosen as the working fluid with (*Pr*) = 0.71.

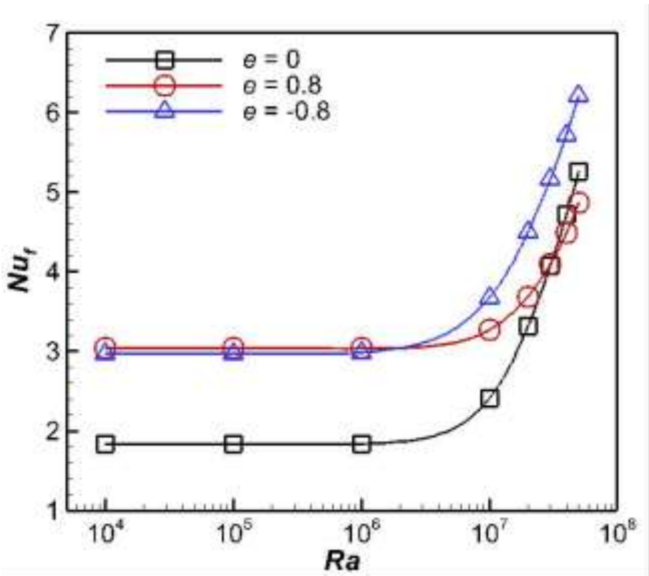

Figure 5. Distribution of average fluid Nusselt number Nu_f against Rayleigh number for various annuli eccentricity.

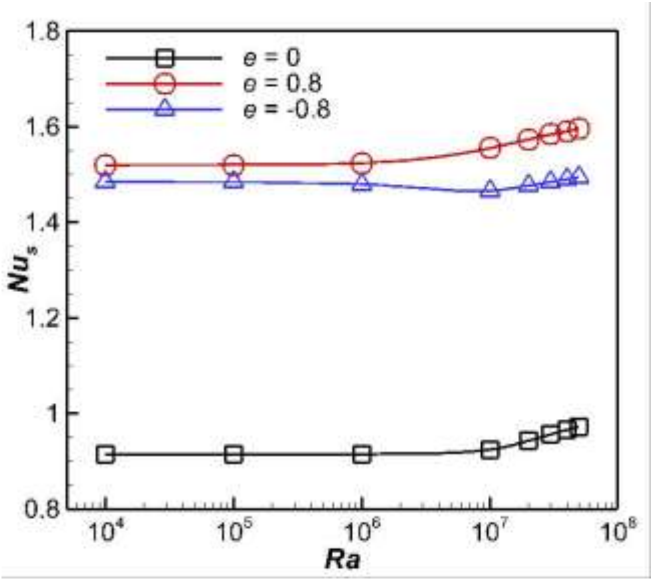

Figure 6. Variation of average solid Nusselt number Nu_s with Rayleigh number for different annuli eccentricity.

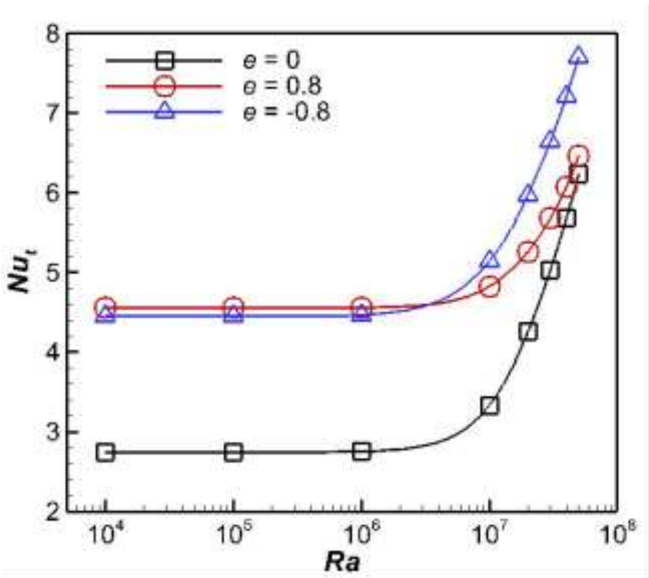

Figure 7. Variation of average total Nusselt number Nu_t with Rayleigh number for different annuli eccentricity.

Re=10^4 *Re*=10^7

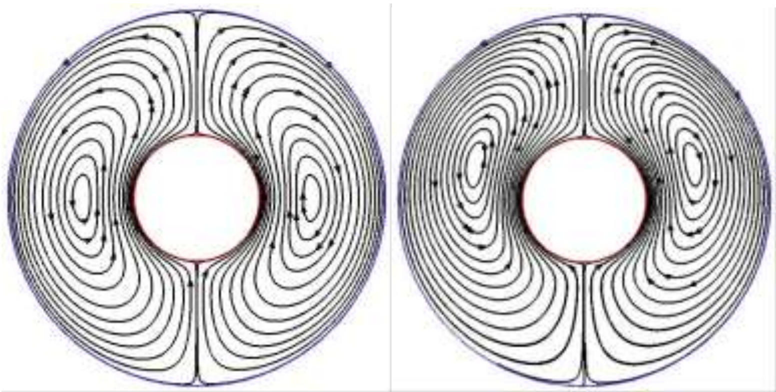

$Re=2\times10^7$ $Re=3\times10^7$

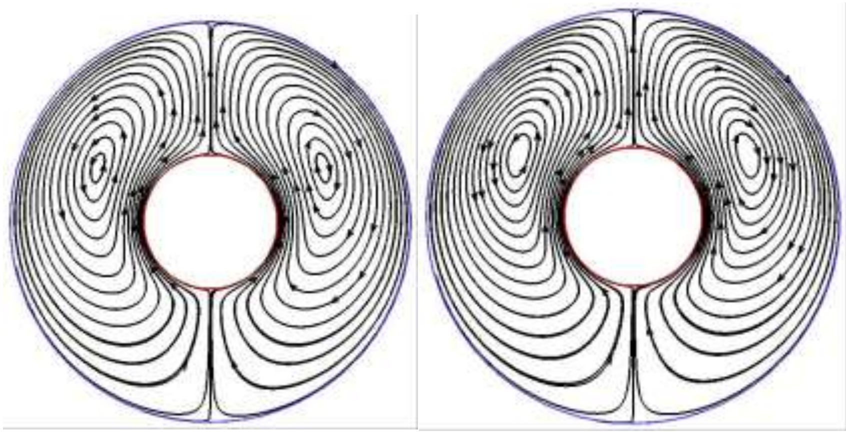

$Re=4\times10^7$ $Re=5\times10^7$

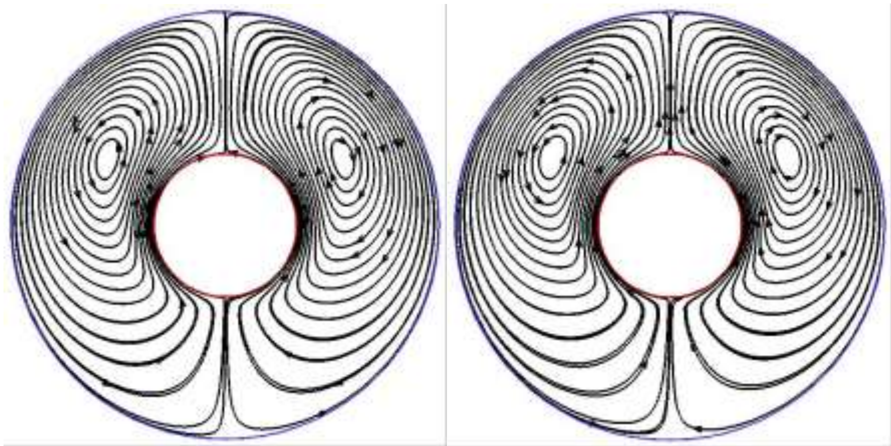

Figure 8. Streamline patterns for buoyancy-induced flow at different Rayleigh numbers for concentric annuli e=0.

$Re=10^4$ $Re=10^7$

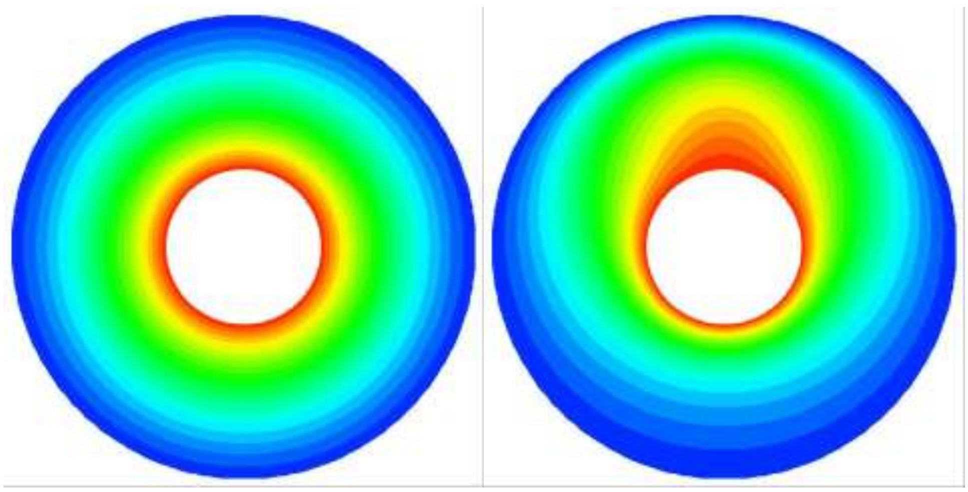

$Re=2\times10^7$ $Re=3\times10^7$

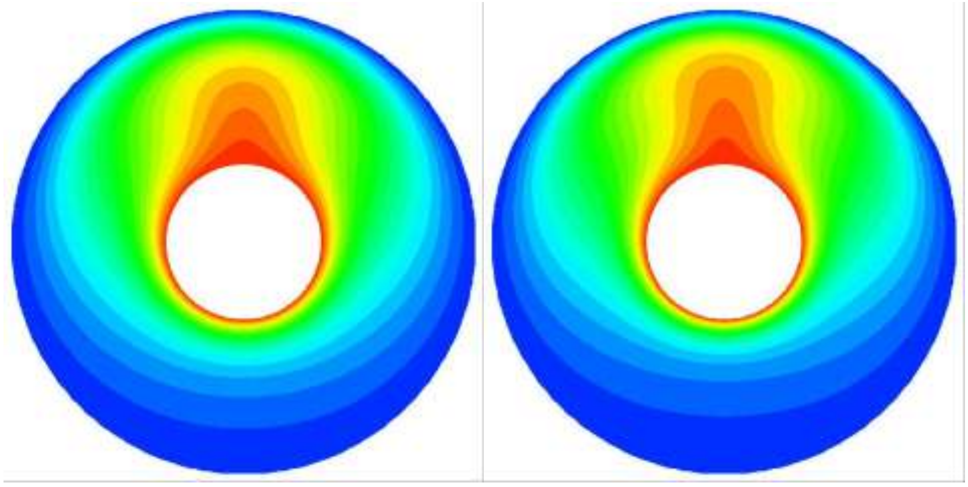

Re=4×10^7 *Re*=5×10^7

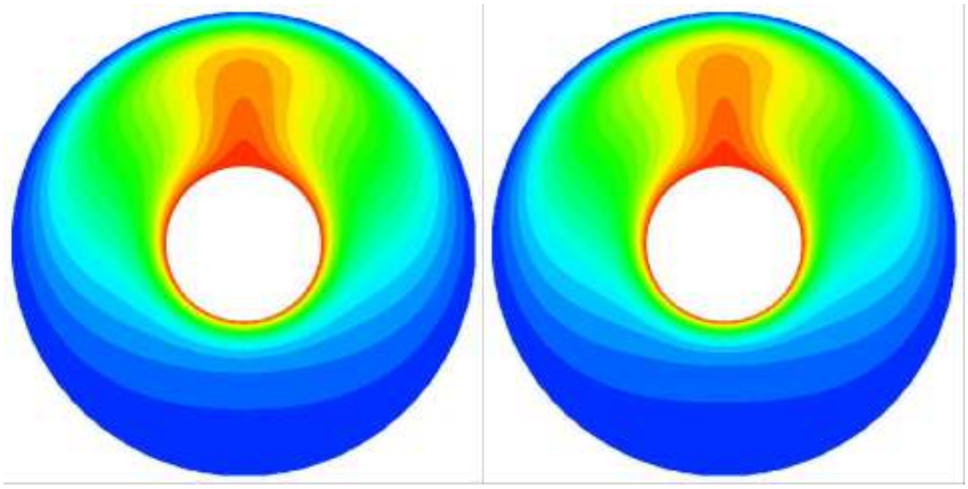

Figure 9. Isotherm patterns for the fluid phase of buoyancy-induced flow at different Rayleigh numbers for concentric annuli *e*=0.

Re=10^4 *Re*=10^7

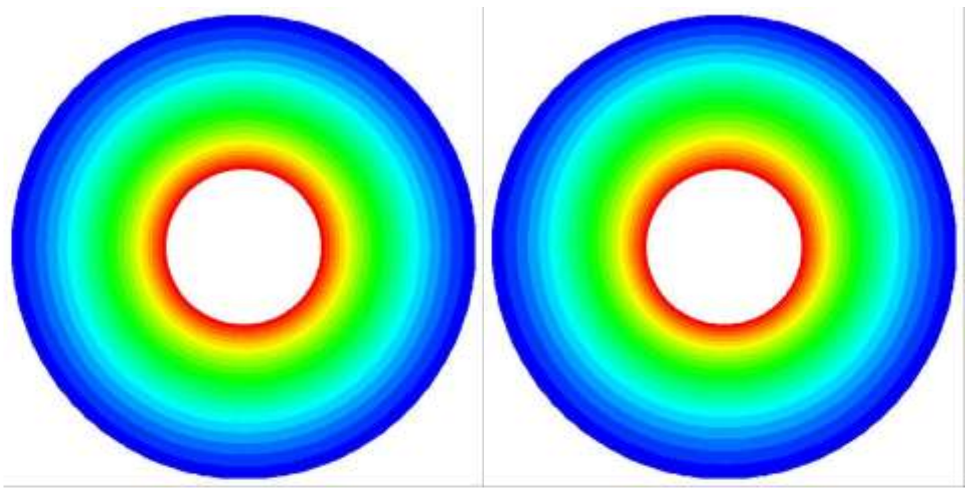

Re=2×10^7 *Re*=3×10^7

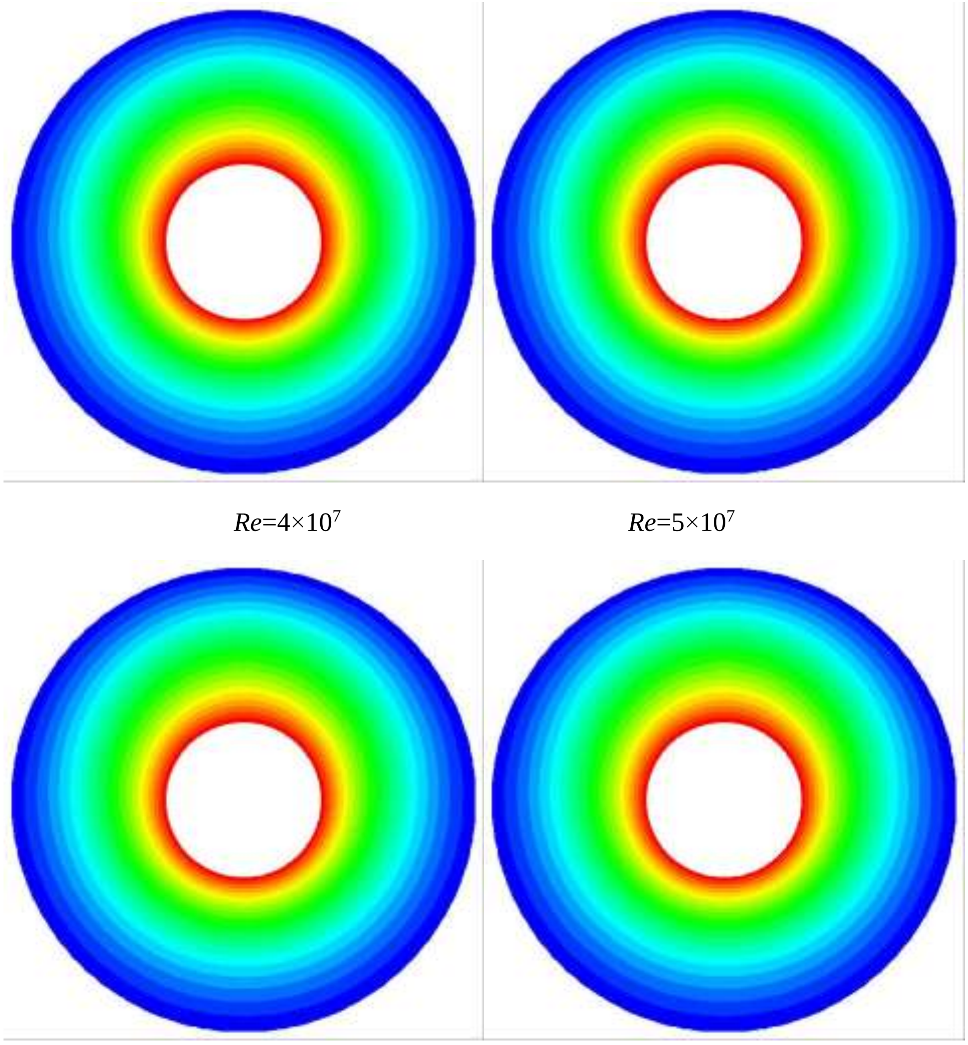

Figure 10. Isotherm patterns for the solid phase of buoyancy-induced flow at different Rayleigh numbers for concentric annuli *e*=0.

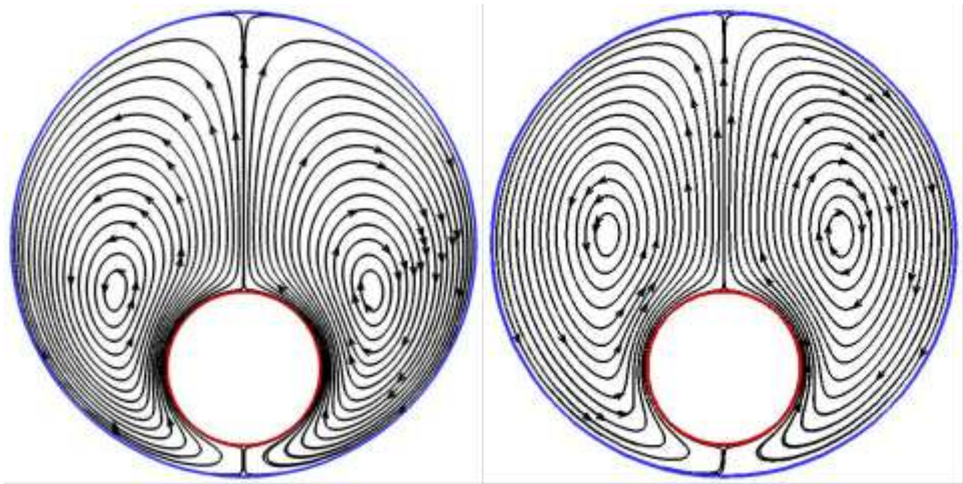

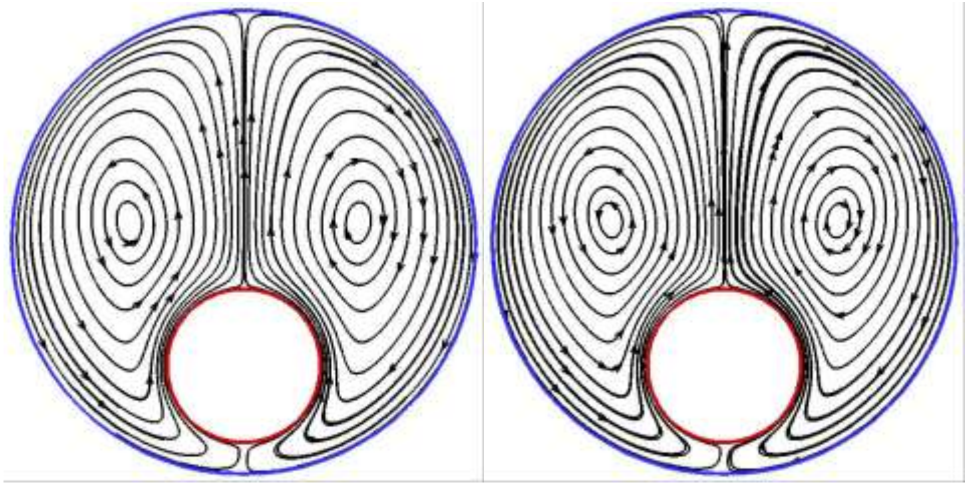

Re=4×10^7 *Re*=5×10^7

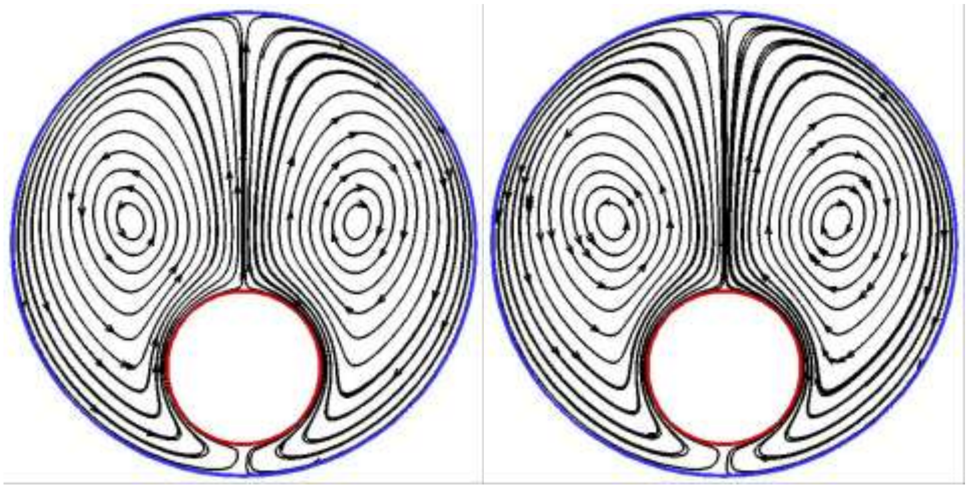

Figure 11: Streamline patterns for natural convective flow at different Rayleigh numbers for eccentric annuli *e*= -0.8.

Re=10^4 *Re*=10^7

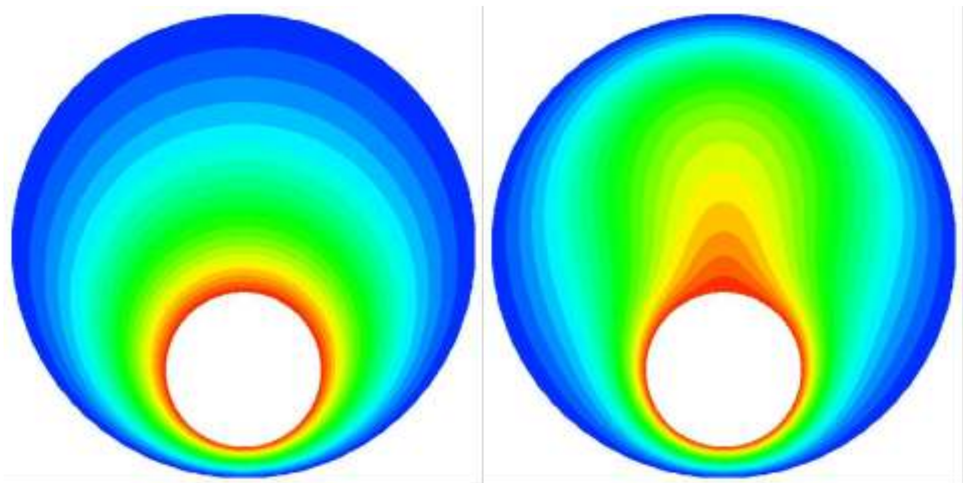

Re=2×10^7 *Re*=3×10^7

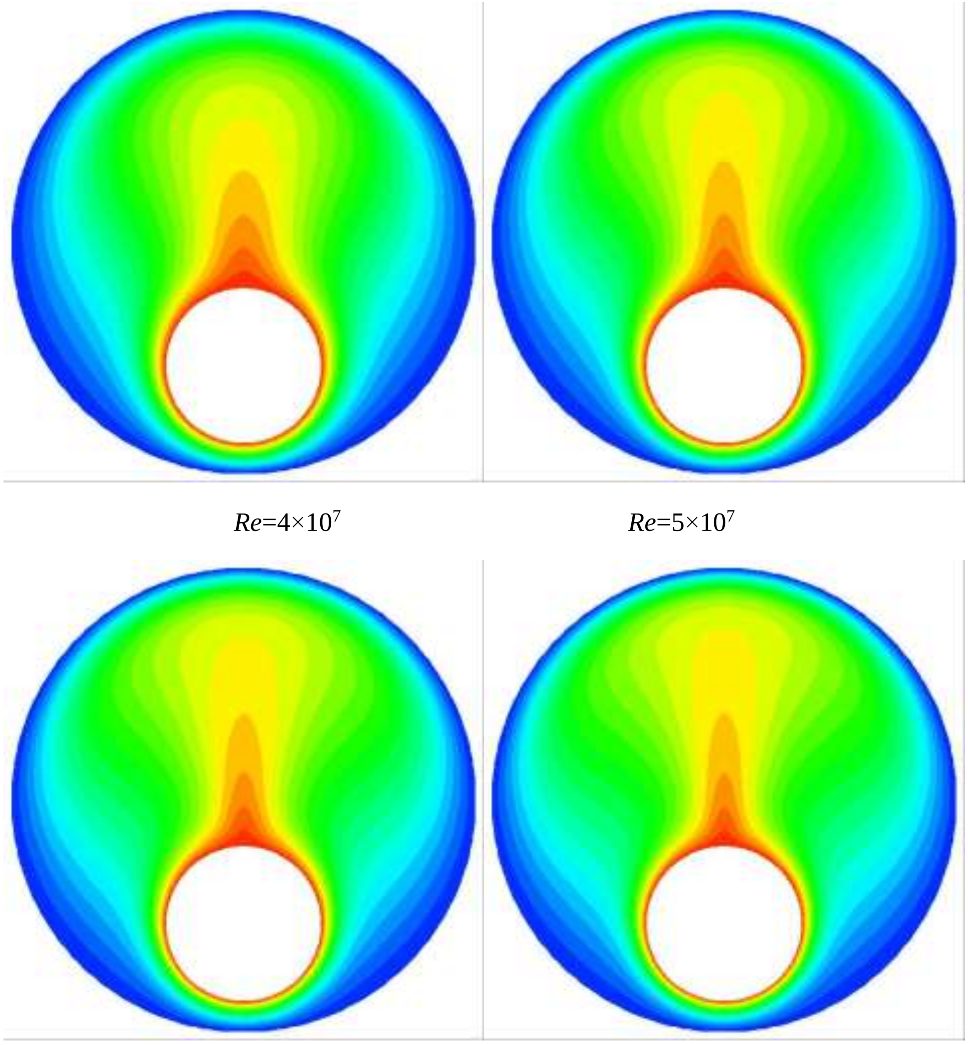

Figure 12. Isotherm patterns for natural convective flow at different Rayleigh numbers for eccentric annuli e= -0.8.

Re=10^{4} Re=10^{7}

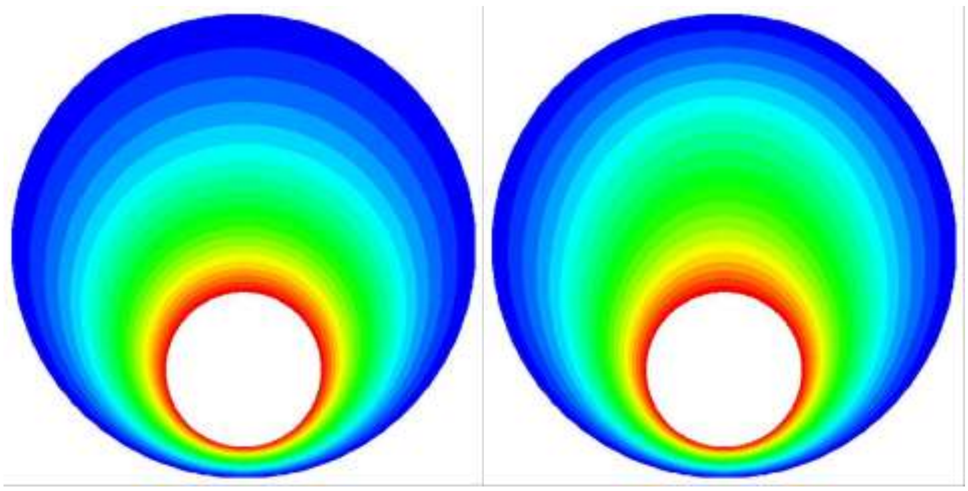

Re=2×10^{7} Re=3×10^{7}

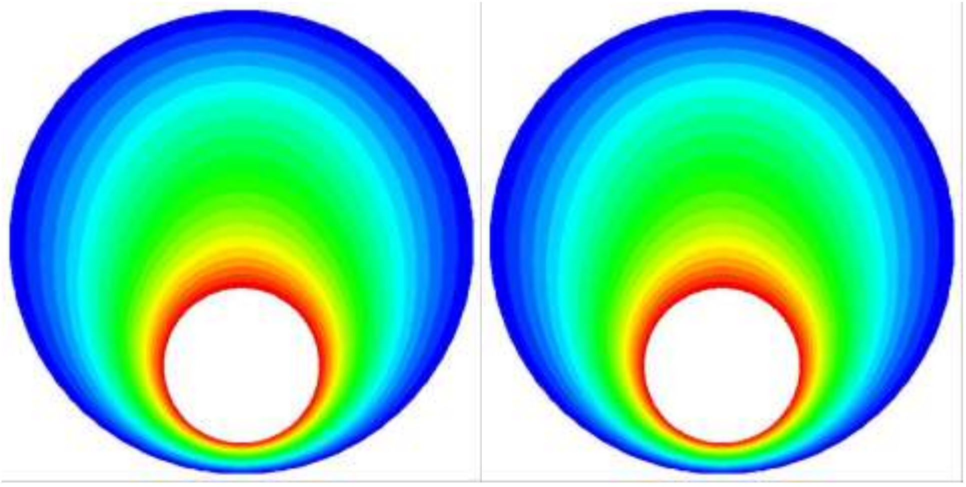

Re=4×10^7 *Re*=5×10^7

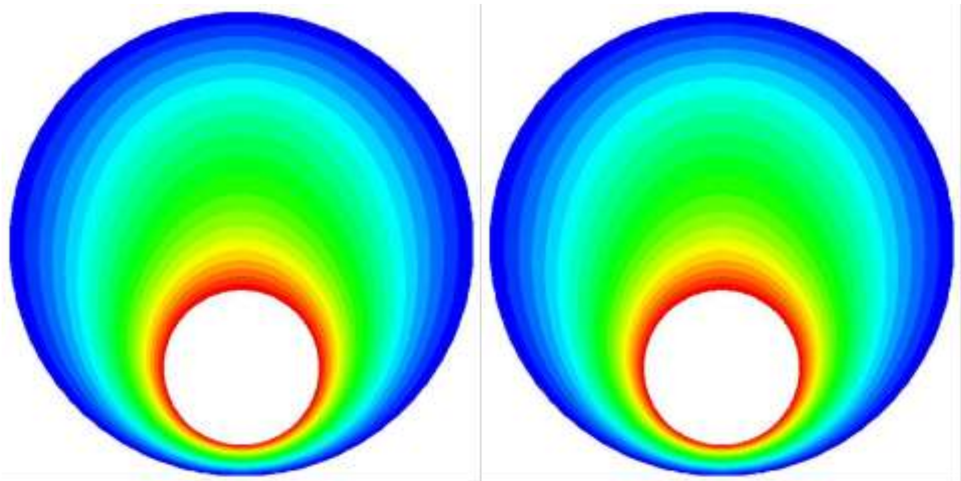

Figure 13. Isotherm patterns for the solid phase of buoyancy-induced flow at different Rayleigh numbers for eccentric annuli *e*=-0.8.

Re=10^4 *Re*=10^7

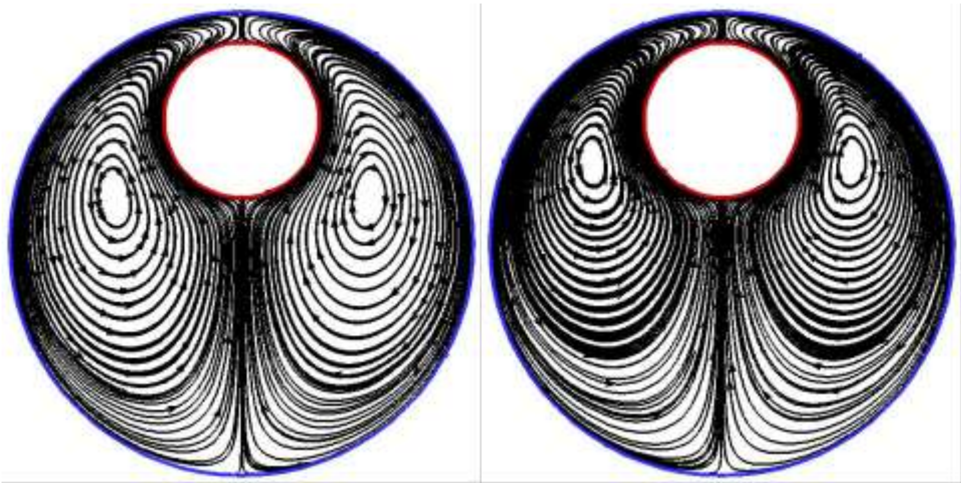

Re=2×10^7 *Re*=3×10^7

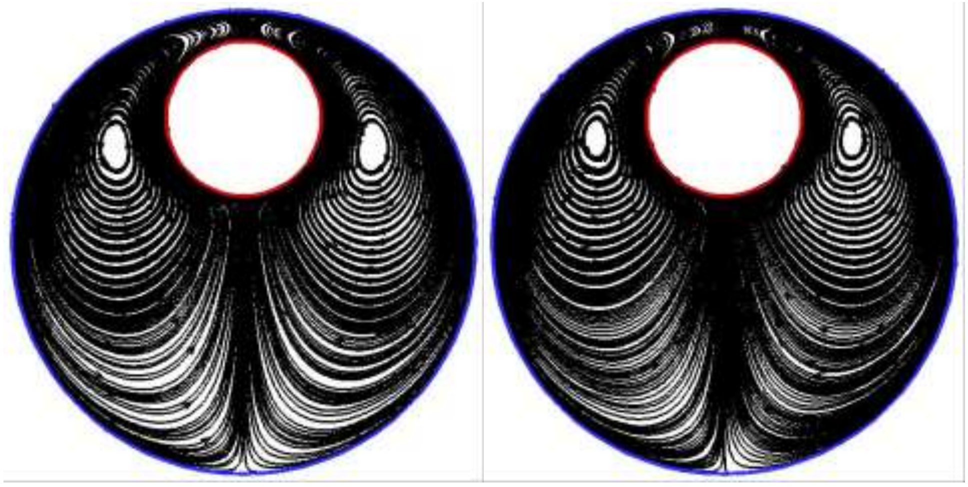

Re=4×10^7 Re=5×10^7

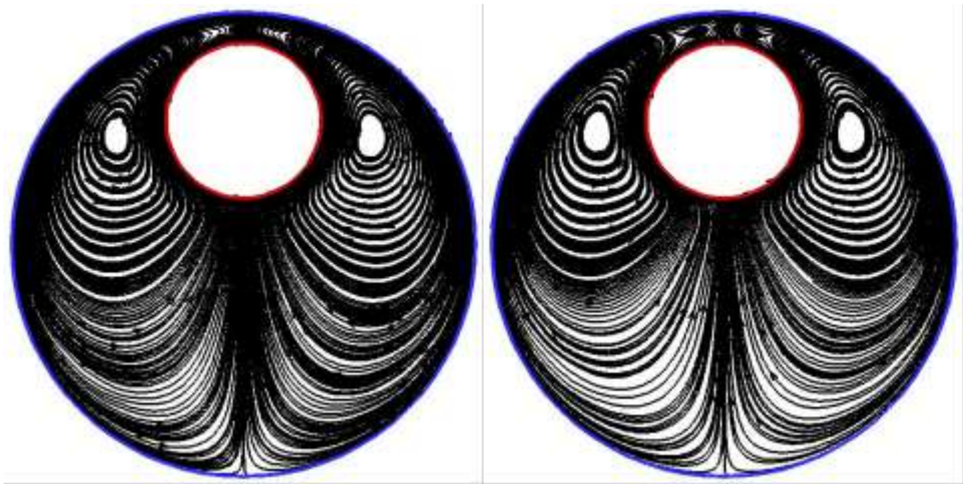

Figure 14. Streamline patterns for natural convective flow at different Rayleigh numbers for eccentric annuli e= 0.8.

Re=10^4 Re=10^7

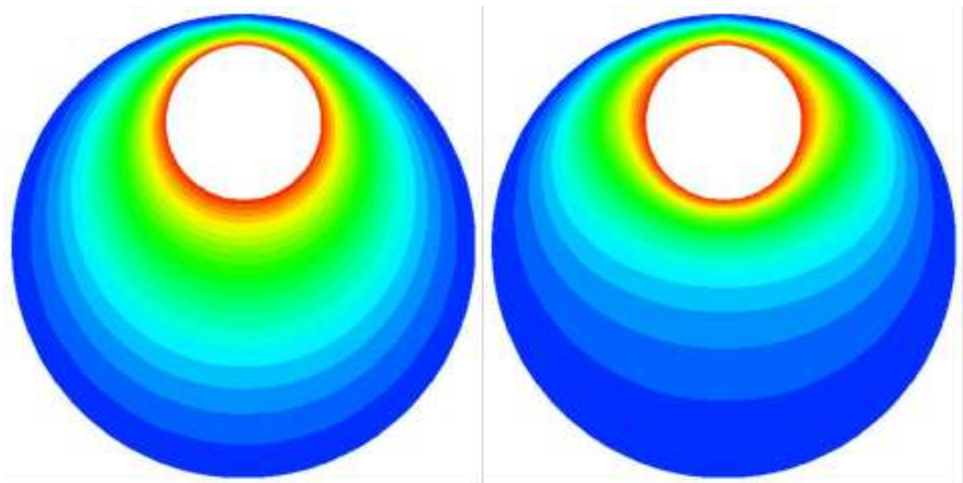

Re=2×10^7 Re=3×10^7

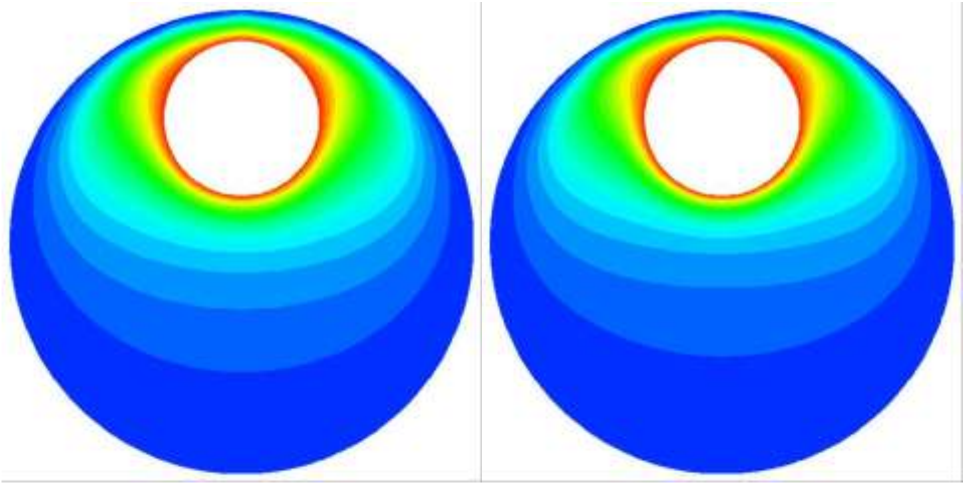

Re=4×10^7 *Re*=5×10^7

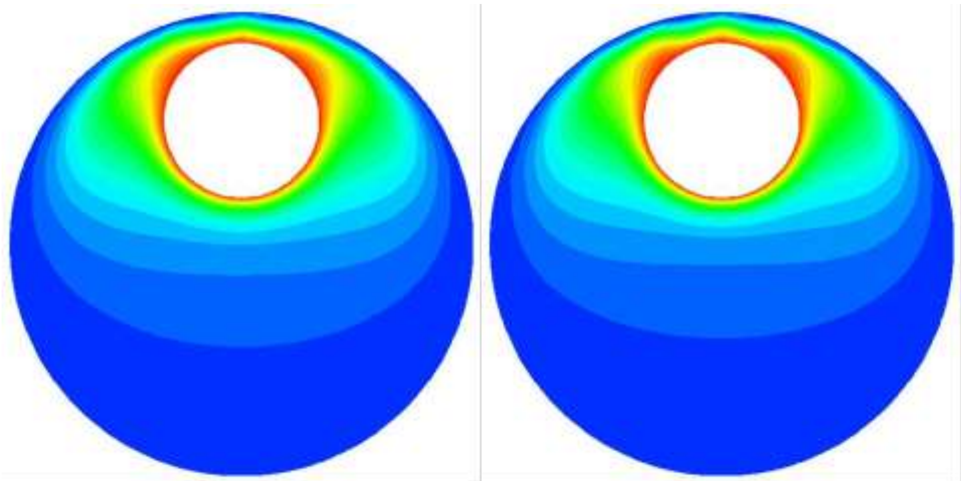

Figure 15. Isotherm patterns for natural convective flow at different Rayleigh numbers for eccentric annuli *e*= 0.8.

Re=10^4 *Re*=10^7

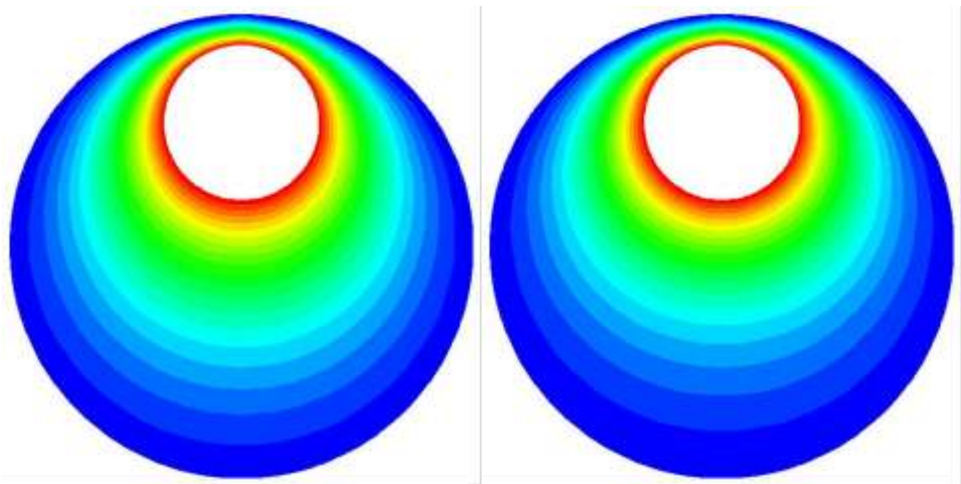

Re=2×10^7 *Re*=3×10^7

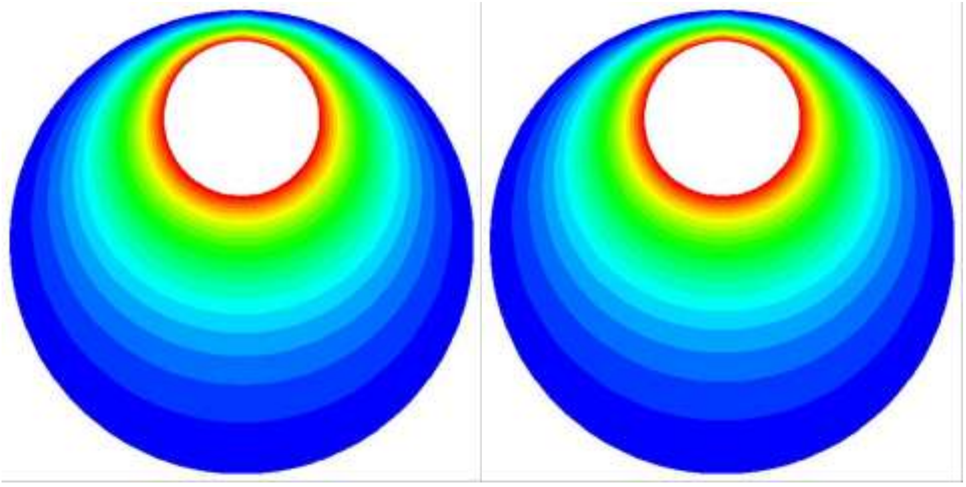

Re=4×10^7 *Re*=5×10^7

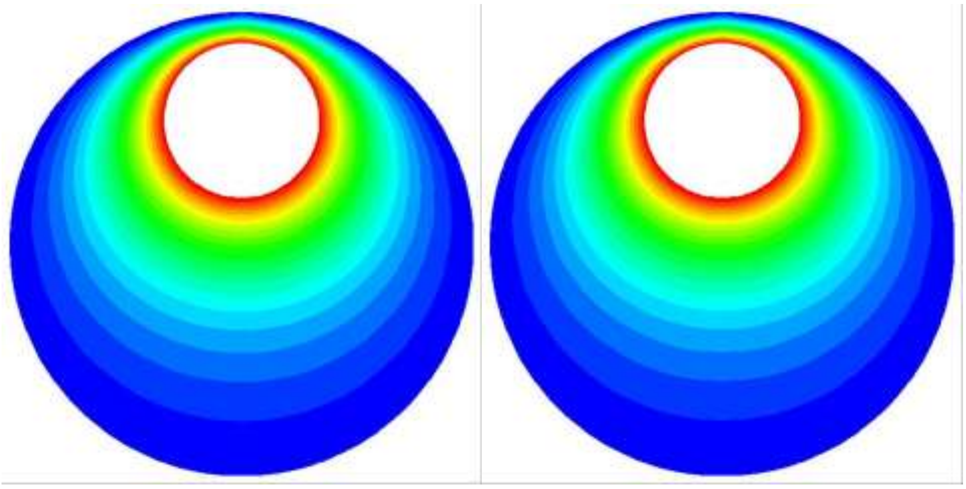

Figure 16. Isotherm patterns for the solid phase of buoyancy-induced flow at different Rayleigh numbers for eccentric annuli *e*=0.8.

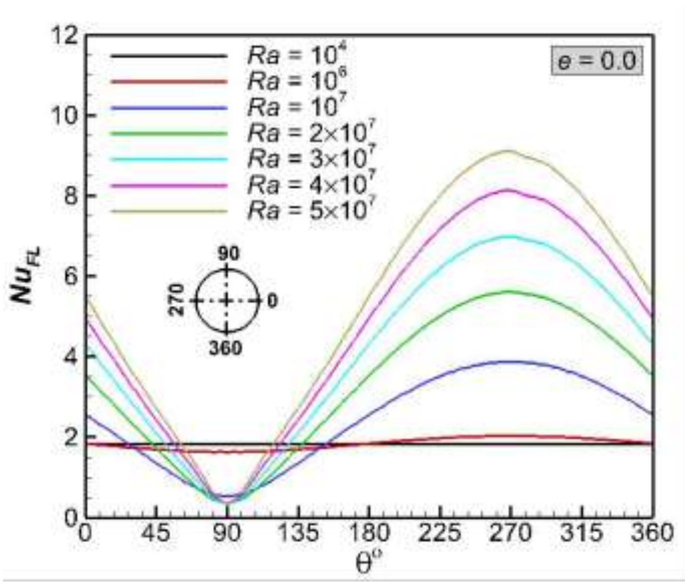

Figure 17. Local fluid Nusselt number distributions along the heated surface of the cylinder at different Rayleigh numbers for concentric annuli *e*=0.

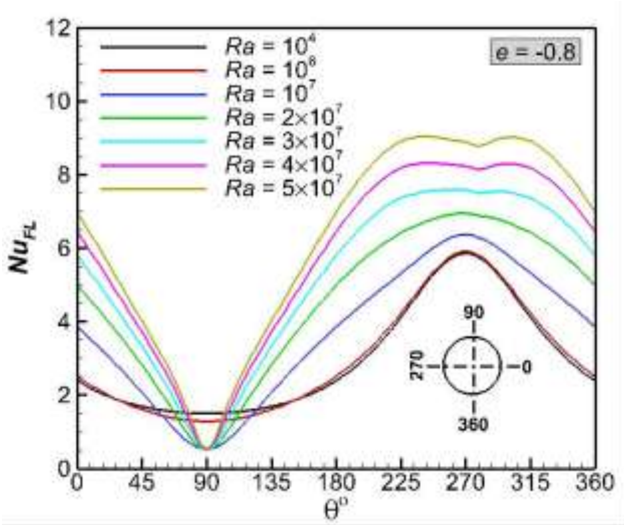

Figure 18. Local fluid Nusselt number distributions along the heated surface of the cylinder at different Rayleigh numbers for eccentric annuli e=-0.8.

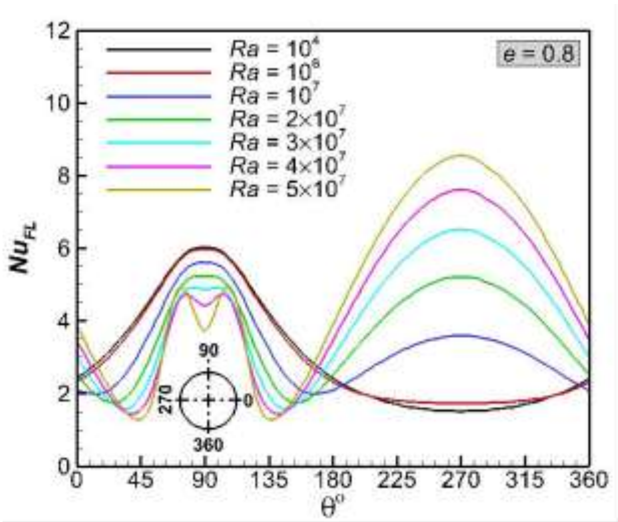

Figure 19. Local fluid Nusselt number distributions along the heated surface of the cylinder at different Rayleigh numbers for eccentric annuli e=0.8.

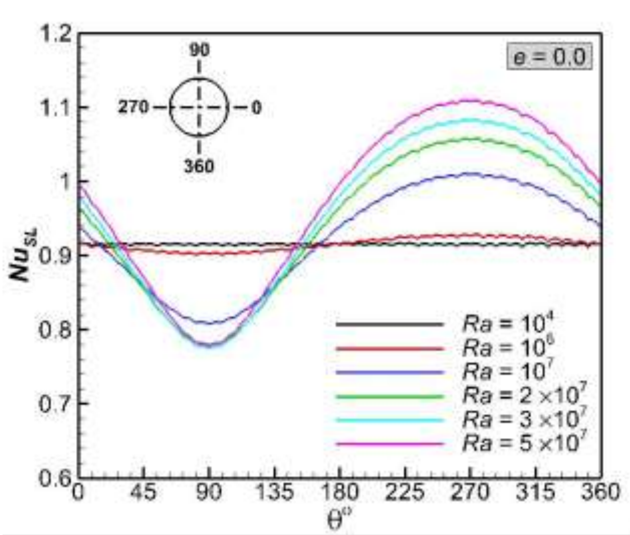

Figure 20. Local solid Nusselt number distributions along the heated surface of the cylinder at different Rayleigh numbers for concentric annuli e=0.

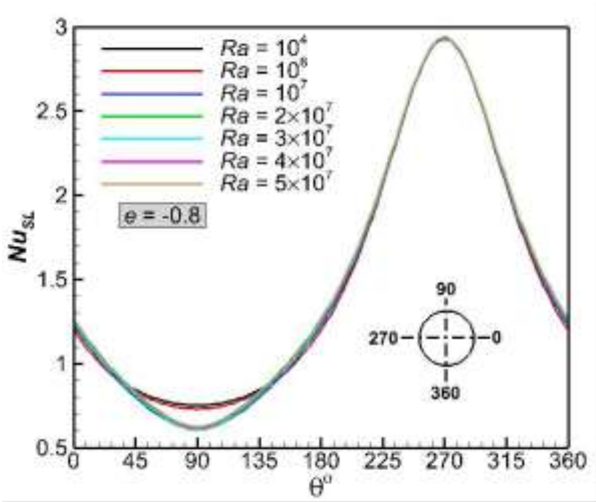

Figure 21. Local solid Nusselt number distributions along the heated surface of the cylinder at different Rayleigh numbers for eccentric annuli e=-0.8.

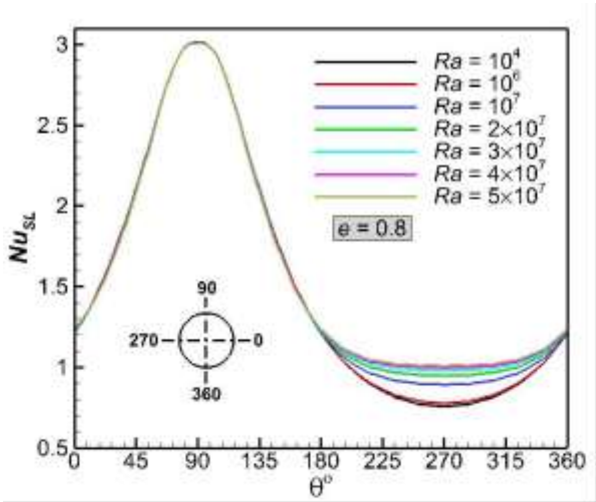

Figure 22. Local solid Nusselt number distributions along the heated surface of the cylinder at different Rayleigh numbers for eccentric annuli e=0.8.

CONCLUSION

The current numerical investigation presents the results for natural convection heat transfer and fluid flow around concentric and eccentric annuli packed with spherical beds using the *LTNE*-local thermal non-equilibrium energy model. The effects of the eccentricity and Rayleigh number on the hydraulic and thermal patterns within the fluid and solid phases, as well as on the local and average fluid and solid Nusselt numbers, Nu_f and Nu_s, respectively, are investigated in detail. The following conclusions are drawn from this study:

1. The thermal and flow characteristics and the heat transfer rates across the annulus is significantly dependent on Ra and e.

2. The increase in Ra generates a considerable increase in Nu_f and a slight increase in Nu_s.

3. Moving the inner cylinder toward the upper region with (e = 0.8) or toward the lower region (e = -0.8), of the outer cylinder causes a great increase in Nu_f for Ra ($\leq 10^6$).

4. Importantly, the maximum increase in Nu_f can be obtained at the higher negative annulus eccentricity e = -0.8 for the higher Ra.

5. The values of the Nu_f seem to be much higher than Nu_s

REFERENCES

[1] T.H. Schwalp, and K.J. de Witt, “Numerical investigation of free convection between two vertical coaxial cylinders”, A.LCh.E. Journal, Vol. 16, Pp. 1005-1010, 1970.

[2] R. Powe, C. Corley, and S. Carrath, “A Numerical solution for natural convection in cylindrical annuli”, Journal of Heat Transfer, 93, Pp. 210-220, 1971.

[3] J.R. Custer, and E.J. Shaughnessy, “Natural Convection in Liquid Metals in an Enclosure”, Journal of Heat Transfer, Vol. 99, Pp. 675-676, 1977.

[4] M.C. Charrier-Mojtabi, A. Mojtabi, and J.P. Caltagirone, “Numerical solution of a flow due to natural convection in horizontal cylindrical annulus”, Journal of Heat Transfer, Vol. 101, Pp. 171-173, 1979.

[5] F. Keivan, G. Atena, S. Nima, and B.M. Hossein, “Simulation of natural convection heat transfer using nano fluid in a concentric annulus”, Thermal Science, Vol. 21, Pp. 1275-1286, 2017.

[6] N.H. Kuehn, and R.J. Goldstein, “Correlating equations for natural convection heat transfer between horizontal circular cylinders”, International Journal of Heat and Mass Transfer, Vol. 10, Pp. 1127-1134, 1976.

[7] A.C. Ratzel, C.E. Hickox, and D.K. Gartling, “Techniques for reducing thermal conduction and natural convection heat losses in annular receiver geometries”, Journal of Heat Transfer, Vol. 101, Pp. 108-113, 1979.

[8] L.S. Yao, “Analysis of heat transfer in slightly eccentric annuli”, Journal of Heat Transfer, Vol. 102, Pp. 279-284, 1980.

[9] V. Projahn, H. Reiger, and H. Beer, “Numerical analysis of laminar natural convection between concentric and eccentric cylinders”, Numerical Heat Transfer, Vol. 4, Pp. 131-146, 1981.

[10] E.E. Feldman, R.W. Hornbeck, and J.F. Osterle, “Numerical solution of laminar developing flow in eccentric annular ducts”, International Journal of Heat and Mass Transfer, Vol. 25, Pp. 131-241, 1982.

[11] W.P. Darrell, and E.C. Roger, “Numerical solution of natural convection in eccentric annuli”, AIAA Journal, Vol. 21, 1983.

[12] J. Ho, Y. H. Lin, and T.C. Chen, “A numerical study of natural convection in concentric and eccentric horizontal cylindrical annuli with mixed boundary conditions”, International Journal of Heat and Fluid Flow, Vol. 10, Pp. 40-47, 1989.

[13] T.H. Hwang, and M.K. Jensen, “An analysis of convective heat transfer to laminar dispersed flow in eccentric annuli”, International communication in Heat and Mass Transfer, Vol. 18, Pp. 27-38, 1991.

[14] H. Koichi, H. Toshitaka, and I. Youji, “Natural convection heat transfer in eccentric horizontal annuli between a heated outer tube and a cooled inner tube with different orientation: The case of an elliptical outer tube”, Heat Transfer Asian Research, Vol. 30, 2001.

[15] R. Hosseini, M.R. Heyrani-Nobari, and M. Hatam, “An experimental study of heat transfer in an open-ended vertical eccentric annulus with insulated and constant heat flux boundaries”, Applied Thermal Engineering, Vol. 25, Pp. 1247-1257, 2005.

[16] J.P. Caltagirone, “Thermoconvective instabilities in a porous medium bounded by two concentric horizontal cylinders”, Journal of Fluid Mechanics, Vol. 76, Pp. 337-362, 1976.

[17] K. Fukuda, Y. Takuta, and S. Hasegawa, “Three-dimensional natural convection in a porous medium between concentric inclined cylinders, in: ASME, Orlando, FL, 1981.

[18] Y.F. Rao, K. Fukuda, and S. Hasegawa, “Steady and transient analyses of natural convection in a horizontal porous annulus with the Galerkin method”, ASME Journal of Heat Transfer, Vol. 109, Pp. 919-927, 1987.

[19] Y.F. Rao, K. Fukuda, and S. Hasegawa, “A numerical study of three-dimensional natural convection in a horizontal porous annulus with Galerkin method”, International Journal of Heat Mass Transfer, Vol. 31, Pp. 695-707, 1988.

[20] K. Himasekhar, and H.H. Bau, “Two-dimensional bifurcation phenomena in thermal convection in horizontal, concentric annuli containing saturated porous media”, Journal of Fluid Mechanics, Vol. 187, Pp. 267-300, 1988.

[21] M.C. Charrier-Mojtabi, A. Mojtabi, M. Azaiez, and G. Labrosse, “Numerical and experimental study of multicellular free convection flows in an annular porous layer”, International Journal of Heat and Mass Transfer, Vol. 34, Pp. 3061-3074, 1991.

[22] J.P.B. Mota, and E. Saatdjian, “Natural convection between two horizontal porous cylinders”, Advanced Computational Methods in Heat Transfer, Vol. 2, Pp. 393-401, 1992.

[23] J.P.B. Mota, and E. Saatdjian, “Natural convection in a porous, horizontal cylindrical annulus”, ASME Journal of Heat Transfer, Vol. 116, Pp. 621-626, 1994.

[24] J.P.B. Mota, and E. Saatdjian, “Natural convection in porous cylindrical annuli”, International Journal of Numerical Methods for Heat and Fluid Flow, Vol. 5, Pp. 3-12, 1995.

[25] H.H. Bau, G. McBlane, and I. Saferstein, “Numerical simulation of thermal convection in an eccentric annulus containing porous media”, in: ASME 32-WA/HT-34, 1983.

[26] H.H. Bau, “Low Rayleigh number thermal convection in a saturated porous medium bounded by two horizontal eccentric cylinders”, Journal of Heat Transfer, Vol. 106, Pp. 166-175, 1984.

[27] K. Himasekhar, and H.H. Bau, “Large Rayleigh number convection in a horizontal, eccentric annulus containing saturated porous media”, International Journal of Heat and Mass Transfer, Vol. 29, Pp. 703-712, 1986.

[28] J.P.B. Mota, and E. Saatdjian, “On the reduction of natural convection heat transfer in horizontal eccentric annuli containing saturated porous media”, International Journal of Numerical Methods for Heat and Fluid Flow, Vol. 7, Pp. 401-416, 1997.

[29] J.P.B. Mota, I.A. Esteves, C.A. Portugal, and E. Saatdjian, “Natural convection heat transfer in horizontal eccentric elliptic annuli containing saturated porous media”, International Journal of Heat and Mass Transfer, Vol. 43, Pp. 4367-4379, 2000.

[30] K. Vafai, and M. Sozen, “Analysis of energy and momentum transport for fluid flow through a porous bed”, Journal of Heat Transfer, Transactions of the ASME, Vol. 112, Pp. 690-699, 1994.

[31] A. Amiri, and K. Vafai, “Analysis of dispersion e_ects and non-thermal equilibrium, non- Darcian, variable porosity incompressible flow through porous media”, International Journal of Heat and Mass Transfer, Vol. 37, Pp. 939-959, 1994.

[32] S. Ergun, “Fluid flow through packed columns”, Chemical Engineering Progress, Vol. 48, Pp. 89-94, 1952.

[33] F.A. Dullien, “Media fluid transport and pore structure”, Academic Press, New York, 1979.

[34] N. Wakao, S. Kaguei, and T. Funazkri, “Effect of fluid dispersion coefficients on particle to fluid heat transfer coefficients in packed beds- correlation of Nusselt numbers”, Chemical Engineering Science, Vol. 34, Pp. 325-336, 1979.

[35] P. Zehner, and E.U. Schluender, “Thermal conductivity of granular materials at moderate temperatures”, Chemie-Ingenieur-Technik, Vol. 42, Pp. 933-941, 1970.

[36] C.A.J. Fletcher, “Computational Galerkin methods”, Springer-Verlag, New York, 1984.

[37] C.A.J. Fletcher, “Computational techniques for fluid dynamics”, Vol. 1, Springer-Verlag, New York, 1991.

[38] G.E. Karniadakis, and S.J. Sherwin, “Spectral/hp methods for computational fluid dynamics”, Oxford University Press, Oxford, 2005.

[39] E. Buyruk, "Numerical study of heat transfer characteristics on tandem cylinders, inline and staggered tube banks in cross flow of air", International Communications in Heat and Mass Transfer, Vol. 29, Pp. 355-366, 2002.

NOMENCLATURE

d	Enclosure inlet slot or outlet vent height, (m).
Gr	Grashof No., $\left(Gr = g.\beta.H^3.(T_w - T_o)/v^2\right)$.
h	Coefficient of local convective heat transfer, (W/m^2.K).
H	Enclosure height, (m).
k	Thermal conductivity, (W/m.K).
N	Number of internal nodes.
Nu_{av}	Temporal surface-average Nusselt no.
Nu_l	Local mean-time surface-average Nusselt no.
Nu_m	Time- and surface-average Nusselt no.
p	Pressure, (N/m^2).
P	Dimensionless pressure, $\left(P = p / \rho.\upsilon_o^2\right)$.
Pr	Prandtl no., $\left(\Pr = v / \alpha\right)$.
Re	Reynolds no., $\left(\mathrm{Re} = \upsilon_o.H / v\right)$.
Ri	Richardson no., $\left(Ri = Gr / \mathrm{Re}^2\right)$.
T	Temperature, (^{o}C).
t	Time, (sec).
u	Horizontal velocity, (m/s).
U	Dimensionless horizontal velocity, $\left(U = u / \upsilon_o\right)$.
υ	Vertical velocity, (m/s).
V	Dimensionless vertical velocity, $\left(V = \upsilon / \upsilon_o\right)$.
x,y	Cartesian coordinates, (m).
X,Y	Dimensionless Cartesian coordinates, (*X* = *x/H*, *Y* = *y/H*).

GREEK SYMBOLS

β	Volumetric expansion coefficient.
θ	Dimensionless temperature, $\left(\theta = (T - T_o)/(T_w - T_o)\right)$.
ρ	Density, (kg/m^3).
v	Kinematic viscosity, (m^2/s).
τ	Dimensionless time.

SUBSCRIPTS

w	Wall
o	Inlet conditions